ORIGINAL ARTICLE

A study of magnetic, antibacterial and antifungal behaviour of a novel gold anchor of polyaniline/ itaconic acid/Fe₃O₄ hybrid nanocomposite: Synthesis and characterization

E. Parthiban [a,b], N. Kalaivasan [c,*], S. Sudarsan [b]

[a] Department of Chemistry, Anna University, Chennai 600025, Tamil Nadu, India
[b] Department of Chemistry, C. Abdul Hakeem College of Engineering and Technology, Melvisharam 632509, Tamil Nadu, India
[c] Department of Chemistry, Thanthai Periyar Government Institute of Technology, Vellore 632002, Tamil Nadu, India

Abstract The objective of the present investigation is to fabricate the gold anchor polyaniline (PANI) based nanocomposites which is prepared using itaconic acid (IA) with Fe₃O₄ by the simple polymerization reaction. The developed multi responsive antibacterial magnetic polymeric composite is represented as Au@PANI–IA–Fe₃O₄. Further, the chemical structure, thermal and magnetic properties such as FT-IR, TGA/DTA, and VSM analysis are studied. The TEM and SEM/EDX are used to find the shape and composition of gold nanoparticles. The enhanced magnetic properties of ferrite composite are exhibited and the antibacterial properties are determined using *E. coli* (gram - ve) and *S. aureus* (gram + ve) bacteria's. The results of biological properties such as antifungal and antimicrobial are also studied critically conferred. Based on the experimental results, the fabrication method of Au@/PANI/IA/Fe₃O₄ magnetic nanocomposites, and the relationship between the structure and biological properties are discussed in detail.

© 2019 The Author(s). Published by Elsevier B.V. on behalf of King Saud University. This is an open access article under the CC BY-NC-ND license (http://creativecommons.org/licenses/by-nc-nd/4.0/).

1. Introduction

Nanotechnology is an effective application in all fields of the research area in modern science. It possesses different shapes and sizes ranging from 1 to 100 nm (Mody et al., 2010). The development of nanotechnology has been significantly accelerated towards the multifunctional nanocomposite materials. Among, several multifunctional nanocomposite materials, those with magnetic and electrical properties are possible aspirants for a wide range of applications such as separation of

biomolecules, biopesticides, bio magnetic separations, biosensors, targeted drug delivery, catalysis, EMI shielding, anticorrosion, anti-biofouling, batteries, supercapacitors, contrast agents in magnetic resonance imaging and electromagnetic device, etc. (Murthy et al., 2002; Wang et al., 2004; Xiao et al., 2018; Geng et al., 2018).

The metallic nanoparticles have shown much attention in recent years because of their different magnetic, catalytic and optical properties. The size, shape, monodispersity, and morphology of the particles have induced these properties (Suganthy et al., 2018; Ibrahim et al., 2017). Several synthesis methods have also been utilized for the preparation of nanoparticle such as chemical, physical, and biological methods, etc. (Khutale and Casey, 2017).

Gold nanoparticles (AuNPs) have been widely used for many applications such as chemical and biological sensing, solar cells, catalysis and biomedical, etc. (Jolanda et al., 2016), infrared radiation absorbing optics (Lee et al., 2008), photothermal therapy and tissue/tumor imaging (Chen and Cui Daxiang, 2012). The biocompatible gold metals possess an effective property against various diseases (Daniel and Astruc, 2004). A substrate for surface improved Raman scattering and catalyst for dye degradation using Water soluble gold-polyaniline nanocomposite (Mondal et al., 2020). They are many researchers attracted gold nanoparticles due to their smaller size, area to volume ratio, higher surface, biocompatible, electrical, optical and catalytic properties (Das et al., 2011).

They are widely used as a post-meal mouth freshener Piper betel Linn (Family: Piperaceae) leaves and crops in India, Malaysia, Sri Lanka, Taiwan, Thailand, and other Southeast Asian countries. The leaves of this plant are economically and medically important in India, China. It has shown excellent antibacterial activity against obligate oral anaerobes responsible for halitosis and it is used to prevent the oral malodorous in Thailand leaves (Ramji et al., 2002). Piper betel leaf has shown an excellent reducing agent in their synthesis in which contains antioxidant and flavonoid compounds. It has been commonly treated as traditional medicine in several Asian countries (Punuri et al., 2012). The part of leaves, roots, stems, stalks, and fruits has been utilized in Piper betel. It has shown large number of biomolecules, such as polyphenols, alkaloids, steroids, tannins, and saponins. The above biomolecules have shown different pharmacological activity viz., carminative, anti-helminthic, stomachic, aphrodisiac, tonic, laxative activities (Khan et al., 2012). Magnetic and superparamagnetic materials have been played an important role in biomedical applications including magnetic resonance imaging for clinical diagnosis, hyperthermia anti-cancer strategy, magnetic drug targeting, etc. (Gupta and Gupta et al., 2005).

Maghemite (Fe_2O_3) and magnetite (Fe_3O_4) were widely used magnetic carriers for a variety of biomedical applications (Liu et al., 2007). Several types of magnetic nanoparticles and their nanocomposites have been prepared in the form of the polymer matrix. However, the number of studies have been done on magnetic polymer nanocomposites such as; polyaniline coated nano-Fe_3O_4/carbon nanotube composite as the protein digestion (Wang et al., 2008), PEI modified Fe_3O_4/gold nanoparticles (sun et al., 2010), alginic acid–Fe_3O_4/nanocomposite (Unal et al., 2010), polyaniline/Fe/Fe_3O_4/Fe_2O_3 nanocomposites with magnetic and optical behavior (Peymanfar et al., 2019), mechanochemically synthesized

Polyaniline/MMT clay nanocomposites (Kalaivasan and Syed Shafi, 2012), superparamagnetic graphene/ polyaniline/ Fe_3O_4 nanocomposites for fast magnetic separation and efficient removal of dye (Mu et al., 2017), silver-anchored polyaniline – chitosan magnetic nanocomposite (Ayad et al., 2017). Li et al has also been revealed the Fe-based metal-organic frameworks of photocatalytic water oxidation catalyst (Li et al., 2019). So, for many researches has also been indicated, the present work based on the purpose of incorporation Fe_3O_4 is to investigate the impact in magnetic conducting polymeric nanocomposite applications (see Table 1).

Itaconic acid (IA) is a multifunctional organic acid and water soluble white crystalline unsaturated dicarbonic acid with two ionisable groups to facilitating to form hydrogen bonds with other side groups (Velickovic et al., 2008). PANI and IA based polymeric materials have shown excellent electrochemical behavior (Barrios et al., 2006). Low-cost and renewable resources by the fermentation with Aspergillus terrus using carbohydrate materials such as molasses and hydrolyzed starch (Isiklan et al., 2010).

Conducting polymers are polymers that have π-conjugated polymeric chains with metal-like electronic, magnetic and optical properties (Ciric-Marjanovic, 2013). The polyacetylene (PAc) in 1976 has also been mentioned on significant material (Heeger, 2001). Conducting polymers has also been exposed such excellent mechanical, tunable properties, good environmental stability, low processing temperature, low cost, solubility, etc. (Mirabedini et al., 2016). Polyaniline is a phenylene-based polymer having –NH– group on either side of the phenylene ring. Aniline is readily undergone oxidative polymerization in the presence of a protonic acid. Protonation has been induced an insulator to conductor transition, while the number of π-electrons in the chain remains constant (Pyarasani et al., 2018). The replacement of metallic conductors and semiconductors with the use of PANI in many applications such as transistors, switches, electrochemical actuators, lithographic resists, lightning protection, microelectronics, solar cells, circuit boards, polymer electrolytes, heating elements, light-emitting diodes (LEDs) electrostatic discharge (ESD), and electromagnetic interference shielding (EMI) applications (Palaniappan and John, 2008). Manawwer Alam et al, has also revealed the optical and electrical conducting behavior of Polyaniline/SnO_2 hybrid nanocomposite (Manawwer Alam et al., 2013). Bifunctional manganese ferrite/polyaniline has been used as a hybrid electrode material for enhanced energy recovery in microbial fuel cell applications (Khilari et al., 2015). Teng et al has also been discussed the applications of supercapacitors based on polyaniline-grafted reduced graphene oxide (Teng et al., 2017). The core–multishell MWCNT/Fe_3O_4/PANI/Au hybrid nanotubes with high-performance electromagnetic absorption material have been fabricated (Liu et al., 2015). Qi et al, also been discussed novel nonenzymatic hydrogen peroxide sensor based on Fe_3O_4/PPy/Ag nanocomposites (Qi et al., 2015). The multifunctional superparamagnetic attapulgite/ Fe_3O_4 /polyaniline nanocomposites have been served as an adsorbent and catalyst (Mu and Wang, 2015). The antibacterial properties of a Polyaniline/polyvinyl alcohol/Ag nanocomposite are prepared (Ghaffari-Moghaddam and Eslahi, 2014). Aniline and 4-Fluoroaniline conducting copolymer composites have been synthesized and doping of silver nanoparticles (Vijayanand et al., 2016). Geng et al were focused on the electrochemical

Table 1 Stoichiometric quantities and physical exterior of Au@PANI-IA-Fe$_3$O$_4$ magnetic nanocomposite based on ANI, IA, and FeCl$_3$ (unit: mol) and PBLE and HAuCl$_4$ solution (unit: mL).

S. No	Sample code	Feed composition					Description
		ANI	IA	FeCl$_3$	PBLE	HAuCl$_4$	
1	GA$_1$I$_3$F$_4$	0.01	0.03	0.04	20	40	Dark blue, insoluble in water
2	GA$_{1.5}$I$_{2.5}$F$_4$	0.015	0.025	0.04	20	40	Dark blue, insoluble in water
3	GA$_2$I$_2$F$_4$	0.02	0.02	0.04	20	40	Dark blue, insoluble in water
4	GA$_{2.5}$I$_{1.5}$F$_4$	0.025	0.015	0.04	20	40	Dark blue, insoluble in water
5	GA$_3$I$_1$F$_4$	0.01	0.04	0.04	20	40	Dark blue, insoluble in water

*Piper betel leaf extract (PBLE).

energy storage and lithium-sulfur batteries applications (Geng et al., 2018, 2019). The Fe$_3$O$_4$/PANI/MnO$_2$ core-shell hybrid has been widely used as adsorbents for the heavy metal ion (Zhang et al., 2017). HCl Doped Au-anchored polyaniline nanocomposites were utilized to study the Electrical, optical and ammonia sensing behavior (Hasan et al., 2015).

The scope of the present investigation to depict the polyaniline/itaconic acid based magnetic nanocomposite by simple route observation with several functionalities. The achieved magnetic nanocomposites have contingent in depth with FT-IR, TGA/DTA, TEM, SEM/EDX, VSM, antibacterial and antifungal studies. In order to examine as nanocomposite, the resultant gold anchor magnetic nanocomposite subjected to different pathogens were parallel to the positive control. The thermal stability of gold anchor magnetic nanocomposites has been decreased upon the concentration of AuNPs. Au@/PANI/IA/Fe$_3$O$_4$ magnetic nanocomposites are very competent biological activity and it is known that the gold anchor itaconic structure manipulate the antibacterial and antifungal efficiency in biological systems. The developed gold anchor magnetic nanocomposites can be useful for medical and industrial applications.

2. Materials and methods

Aniline, Itaconic acid (IA), HAuCl$_4$ were purchased from Sigma Aldrich Company, Bangalore, India. Anhydrous FeCl$_3$ 98% (SISCO, India), ammonia (25% solution), hydrochloric acid (HCl), sodium hydroxide (NaOH) were obtained from Merck Chemicals, India. Solvents grade such as THF, NMP (Merck), Acetone (Sigma Aldrich) Ethanol (SRL) were used in the present work. Fresh leaves of Piper betel were collected from the local market of Vellore, India. Double distilled water was used throughout the experiments without further purification.

2.1. Synthesis of PANI

2 mL (0.02 mol) of aniline monomer was dissolved in 50 mL of 0.1 M HCl with stirring till complete dispersion and homogeneity of solution. Anhydrous FeCl$_3$ (3.5 g) dissolved in 50 mL of distilled water was added dropwise to aniline solution with constant stirring for 5 h. The resulting intermediate PANI was washed several times by double distilled water followed by methanol. The final product was dried in a vacuum oven at 50 °C for 24 h (Ayad et al., 2012).

2.2. Synthesis of PANI–IA–Fe$_3$O$_4$ nanocomposite

Initially, 2.70 g of IA (0.02 mol) was dissolved into 50 mL of double distilled water and stirred for 30 min then 2 mL (0.02 mol) of aniline monomer also added. The resulting solution was left constant under stirring for 1 h to obtained homogenize compound. In an ice bath, 6.5 g (0.04 mol) of anhydrous FeCl$_3$ was added to the mixture and left under mechanical stirring overnight. The sodium hydroxide solution was added slowly to the mixture and maintain the temperature at 10 °C. The resulting product was collected and washed several times with double distilled water and ethanol. The obtained product was dried in an oven at 50 °C for 24 h.

2.3. Preparation of piper betel leaf extract

The piper betel leaves were collected and washed several times with double distilled water. 30 g of piper betel leaves were cut in to a small pieces and put it into a conical flask containing 300 mL double distilled water. The whole content was boiled for about 15 min and filtered through Whatmann filter paper. The obtained extract of leaves was stored at refrigerator at 4 °C till further use of the compound (Punuri et al., 2012).

2.4. Synthesis of gold nanoparticles

A single-step reduction was used to synthesis of AuNPs (Zhan et al., 2011). Briefly, 40 mL of HAuCl$_4$ (1 mM) was prepared and 20 mL of leaf extract was then added to the solution with constant stirring for 2 h. The formation of AuNPs could be indicated by the change of solution color to be a typical dark-red solution. The feed composition of gold anchor Au@PANI-IA-Fe$_3$O$_4$ magnetic nanocomposites shown in Table 2.

2.5. Synthesis of Au nanoparticles @PANI– IA–Fe$_3$O$_4$ nanocomposite

The prepared PANI–IA–Fe$_3$O$_4$ nanocomposite was added to 50 mL of 0.5 M NH$_4$OH for complete deprotonation and then washed using double distilled water. 0.5 g of the previously deprotonated PANI–IA–Fe$_3$O$_4$ nanocomposite was added to 40 mL of AuNPs solution under constant mechanical stirring for 4 h. The obtained product was washed with double distilled water with ethanol several times. The collected final product was dried at room temperature for 3 days for further

Table 2 Solubility result of PANI, PANI–IA–Fe$_3$O$_4$, and Au@PANI–IA–Fe$_3$O$_4$ magnetic nanocomposite.

Name of the Solvent	PANI	PANI–IA–Fe$_3$O$_4$	Au@ PANI–IA–Fe$_3$O$_4$
Ethyl alcohol	IS	IS	IS
Chloroform	SS	IS	IS
Acetic acid	MS	IS	IS
Actone	MS	IS	IS
Dimethyl formamide (DMF)	MS	IS	IS
Dimethyl sulphoxide (DMSO)	MS	IS	IS
Diethylene glycol (DEG)	IS	IS	IS
Tetra hydrocarbon (THF)	SS	IS	IS
THF/water	S	S	S
NMP/water	S	S	S
Double distilled water	IS	IS	IS

*Where S–soluble, MS–mostly soluble, SS–slightly soluble and IS–insoluble.

characterization. The schematic representation of the development of Au@ PANI–IA–Fe$_3$O$_4$ nanocomposite has shown in Scheme 1.

3. Characterization

The FT-IR studies of powdered specimens were recorded on FTIR-8400 S, Shimadzu spectrophotometer. Thermal analysis was carried out using SDT Q600 DTA-TGA to find thermal properties of the magnetic nanocomposite. TGA was measured in the temperature range of 800 °C at a heating rate of 20 °C/min under N$_2$ atmosphere. The XRD patterns of the prepared samples were measured by an X-ray diffractometer (GNR APD-2000 PRO) with CuK a radiation (40 kV, 30 mA) in the step scan mode. Scanning electron microscopy (SEM) images were captured on Tescan Mira 3 LMH at accelerating voltage of 30 kV. Prior to SEM analysis, the samples were freeze dried and kept in vacuum for silver sputtering treatment. Energy-dispersive X-ray (EDX) spectroscopy analysis was done for confirming the presence of iron and gold nanocomposites. Transmission electron microscopy (TEM) was carried out using JEM 2000 and a source of this instrument LaB6 with resolution point 0.23 nm and voltage is 200 kV. Magnetic properties were measured by vibrating sample magnetometer (VSM) on the physical property measurement system (Quantum Design).

3.1. Antibacterial activity

The antibacterial activity of magnetic nanocomposites was evaluated against *Staphylococcus aureus* (gram +ve) and *Escherichia coli* (gram −ve) pathogens spread on Mueller-Hinton agar (MHA) plates. A well of diameter 6 mm was made using a sterile cork borer and loaded with the required concentration sample over the agar. The test plates were incubated for 24 h at 37 °C. The zone of inhibition (mm in

diameter) activity were observed against the test pathogens, Ciproflaxin (20 µg) was used as a positive control.

3.2. Antifungal activity

To estimate the impacts of antibiotic unloaded Au@PANI–IA–Fe$_3$O$_4$ nanocomposites on *Aspergillus niger* and *Candida albicans* growth were analysed by well diffusion method. Petri plates were also been used to prepare 20 mL of sterile MHA (Hi- media, Mumbai). The test culture was washed on the top of solidified media and then allowed to dry for 10 min. Wells were prepared in the media using a well borer. The different concentrations of the samples (50, 100, 250 and 500 µg per well) were loaded on the wells. Ciproflaxin (20 µg/well) used as a positive control. These plates were incubated at 37 °C for 24 h in closed condition. The zone of inhibition was noticed in millimeters (mm).

4. Results and discussion

4.1. Fourier transform infrared spectroscopy (FT-IR) studies

FT-IR spectra tool has been utilized to finding the chemical structure of PANI, IA, PANI–IA–Fe$_3$O$_4$ nanocomposite of before and after anchoring the AuNPs. Fig. 1 has shown the comparison of FT-IR spectra of PANI (Fig. 1a) and IA (Fig. 1b) through the FT-IR spectra of PANI–IA–Fe$_3$O$_4$ (Fig. 1c) and Au@PANI–IA–Fe$_3$O$_4$ (Fig. 1d). The formation of PANI (Fig. 1a) has been confirmed by the characteristics peaks at 1553 cm^{-1} and 1447 cm^{-1} corresponds to C=C stretching of quinonoid and benzenoid respectively (Sampreeth et al., 2018). The sharp peaks at 1315 cm^{-1} and 1221 cm^{-1} was assigned to the C—N stretching vibration in (Q-B-Q) unit and vibration of the secondary aromatic amine. The sharp peaks were observed at 1095 cm^{-1} and 850 cm^{-1} could be assigned to in plane C—H stretching vibration and out of plane C—H bending stretching vibrations respectively (Ayad et al., 2017).

A broad peak has been notified at 3011 cm^{-1}, which is due to O—H stretching vibrations of IA. The (Fig. 1b) sharp peaks have been observed at around 1686, 1431 and 1213 cm^{-1}, indicating the stretching vibrations such as C=O (carboxylic acid), C—O—H in-plane and C—O, respectively. Fig. 1c showed an overlapped peak at 3163 cm^{-1} and 2630 cm^{-1} which is due to the interaction between the PANI and IA. It leads to form PANI–IA–Fe$_3$O$_4$. A new peak has been noticed at 1639 cm^{-1} corresponds to PANI–IA–Fe$_3$O$_4$ nanocomposite which is confirms the disappearance peaks. The peak at 1686 cm^{-1} was also observed in the interaction between PANI and IA Fig. 1c (Zeghioud et al., 2015).

Except for the two peaks at 1300 cm^{-1} and 825 cm^{-1}, other characteristic absorption peaks in the infrared spectrum of the IA doped polyaniline have shown redshift with a broader shape undoped one. The other stretching vibrations such as 1576 cm^{-1}, 1396 cm^{-1} and 1161 cm^{-1} of quinone and benzene rings of C-N stretch in a secondary aromatic amine has been observed. The redshift might be due to the delocalization of positive charge from the imine nitrogen atom to the benzene ring and decrease the electronic interaction intensity. The new absorption peak has been observed at 1238 cm^{-1} which
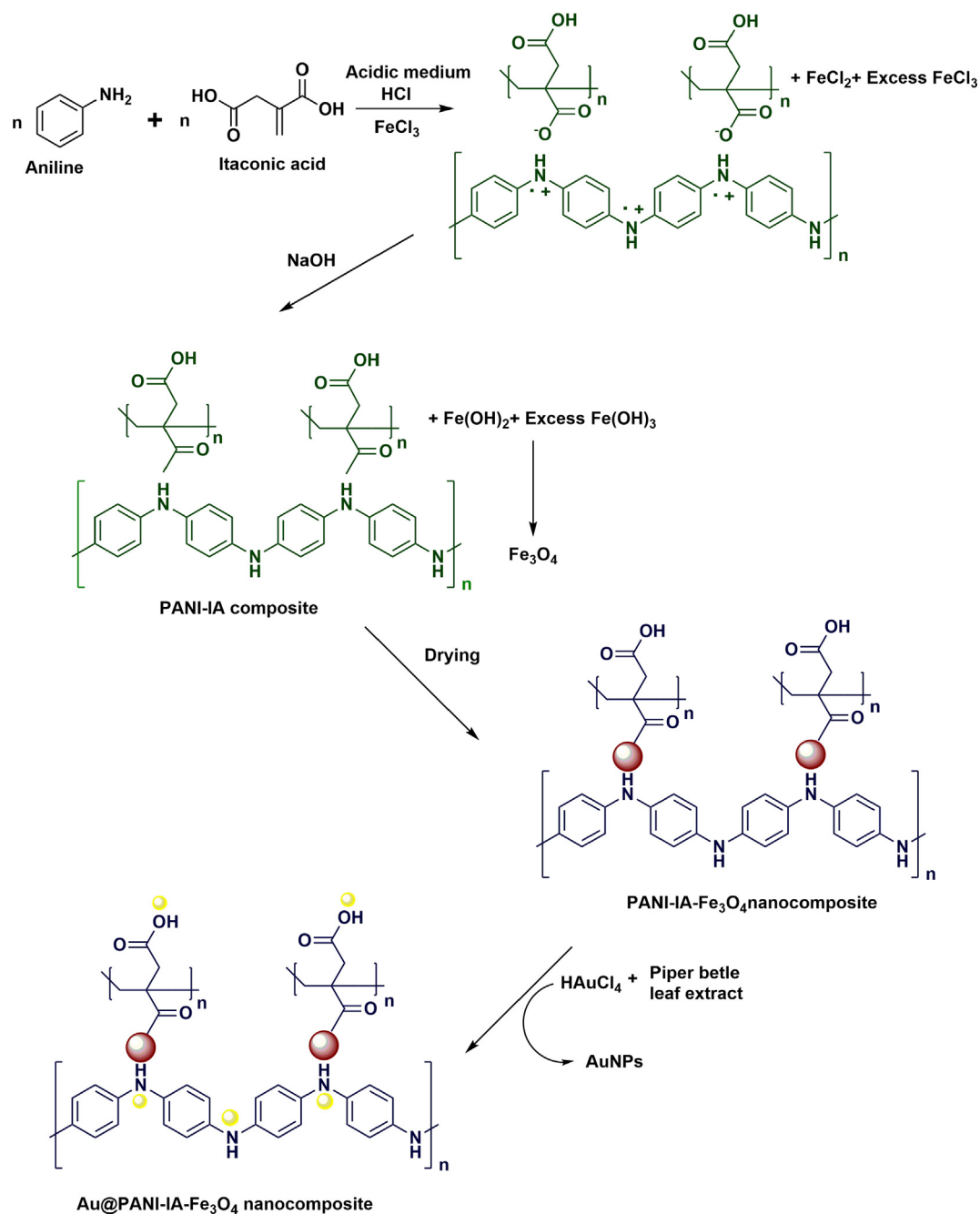
Scheme 1 Shows the schematic representation of Au@PANI–IA–Fe$_3$O$_4$ nanocomposites.

is indicates the doped polyaniline in the nanocomposite (Wang et al., 2014).

The two peaks at 580 cm^{-1} and 464 cm^{-1} has shown the association of pristine magnetite. In Fig. 1c has shown the new appearance of peaks at 553 cm^{-1} and 445 cm^{-1} which well support the presence of magnetite (vibrational Fe—O bond). The shifting of the magnetite peaks from the parent peak exposed to the interaction of magnetite with PANI and IA. A small shift of NH and OH stretching vibration has been noticed in the position at 1639 cm^{-1} and 3263 cm^{-1} (Fig. 1c) to 1608 cm^{-1} and 3246 cm^{-1} (Fig. 1d) which is due to gold metal reduction and its deposition over PANI–IA–Fe$_3$O$_4$ nanocomposite. Hence, this FT-IR gold anchor PANI–IA

magnetic nanocomposites has been well supporting the structure of Au@ PANI–IA–Fe$_3$O$_4$ nanocomposites. Therefore, FT-IR suggest good interaction between IA and PANI with the presence of magnetite and gold nanoparticles on the PANI–IA–Fe$_3$O$_4$ nanocomposite (Peymanfar et al., 2019; Ayad et al., 2017).

4.2. Thermal analysis

Thermal properties of the developed magnetic nanocomposites were examined by the TGA thermogram method. The magnetic nanocomposites such as PANI–IA–Fe$_3$O$_4$ and
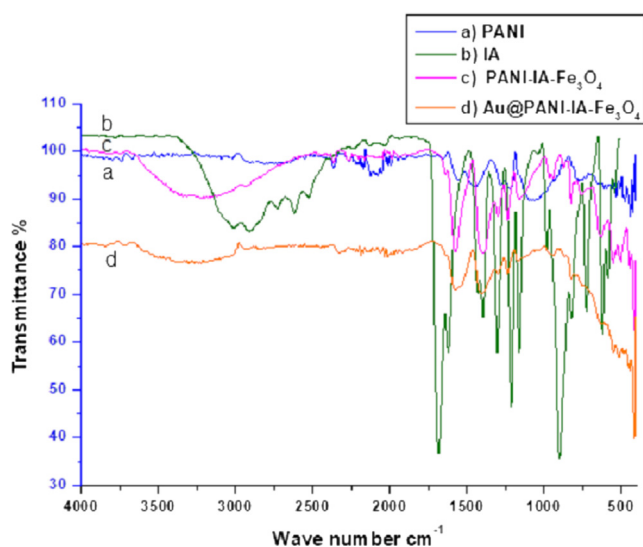
Fig. 1 FTIR spectra of (a) PANI, (b) IA, (c) PANI–IA–Fe$_3$O$_4$ nanocomposite and (d) Au@PANI–IA–Fe$_3$O$_4$ magnetic nanocomposite.

Au@PANI–IA–Fe$_3$O$_4$ has shown in Fig. 2. The different stages of thermal degradation of these materials could be observed as a multistep process. The three-stage weight loss behavior has been noticed due to the evaporation of the humidity or expulsion of water, residual solvents and small molecule form PANI at 40 °C to 150 °C and 40 °C to 325 °C could be attributed to the loss of bounded water moieties and dopant. The samples (a) and (b) an amount of weight loss due to the evolution of water are 21.94% and 30.60% composites cleavages respectively. The second stage of weight loss observed from 150 °C to 545 °C and 325 °C to 500 °C is typical for the degradation of IA. The samples (a) and (b) an amount of weight loss owing to the evolution of the dopant molecules are 10.86% and 27.14% composites, respectively. The third stage of weight loss has been examined between

545 °C and 780 °C and 500 °C to 780 °C which is due to the decomposition of PANI polymer matrix. The complete decomposition of the composite occurred at 780 °C. The samples (a) and (b) an amount of weight loss due to the evolution of water are 28.25% and 16.34% composites, respectively. The total weight loss is about 61.05% and 74.07%, thus the residue of Fe$_3$O$_4$ is about 38.95% and 25.93%. The above percentage was close to the presence of Fe content. The addition of itaconic acid which enhances the thermal stability of magnetic nanocomposite such as PANI–IA–Fe$_3$O$_4$ and Au@PANI–IA–Fe$_3$O$_4$ (Mu et al., 2017; Minisy et al., 2018). Differential analysis (DTA) curve for PANI–IA–Fe$_3$O$_4$ (Fig. 2a) has been observed an endothermic peak at 50 °C to 120 °C and an exothermic peak at 320 °C to 390 °C. The endothermic peak for removal of moisture and water molecule and exothermic for crosslinking of a polymeric matrix with metal and sharp endothermic peak 700 °C to 720 °C has also observed. Similarly, the DTA curve for Au@PANI–IA–Fe$_3$O$_4$ (Fig. 2b) has been noticed an endothermic peak at 70 °C to 120 °C due to the traces amount of water molecules. The exothermic peak at 390 °C to 420 °C has been observed and it is due to the crosslinking of a polymer and strong binding of AuNPs. A small peak at 690 °C has also been observed.

4.3. Solubility analysis

The solubility test was performed in PANI, PANI–IA–Fe$_3$O$_4$ and Au@PANI–IA–Fe$_3$O$_4$ nanocomposite using different organic solvents such as ethyl alcohol, chloroform, acetic acid, DMF, DMSO, DEG, THF, THF/water, NMP/water, hot water, and distilled water. The FT-IR spectra were used for qualitative recording before and after their submerging of organic solvents for 5 min. By comparing these FT-IR spectra for each polymer. The intensities of the FTIR peaks of poly (aniline), PANI–IA–Fe$_3$O$_4$ and Au@PANI–IA–Fe$_3$O$_4$ nanocomposites were observed. The results indicate that the 50% solubility was obtained in organic solvents for polyaniline, whereas 100% solubility was noticed in PANI–IA–Fe$_3$O$_4$. PANI based synthetic nanocomposite were soluble in
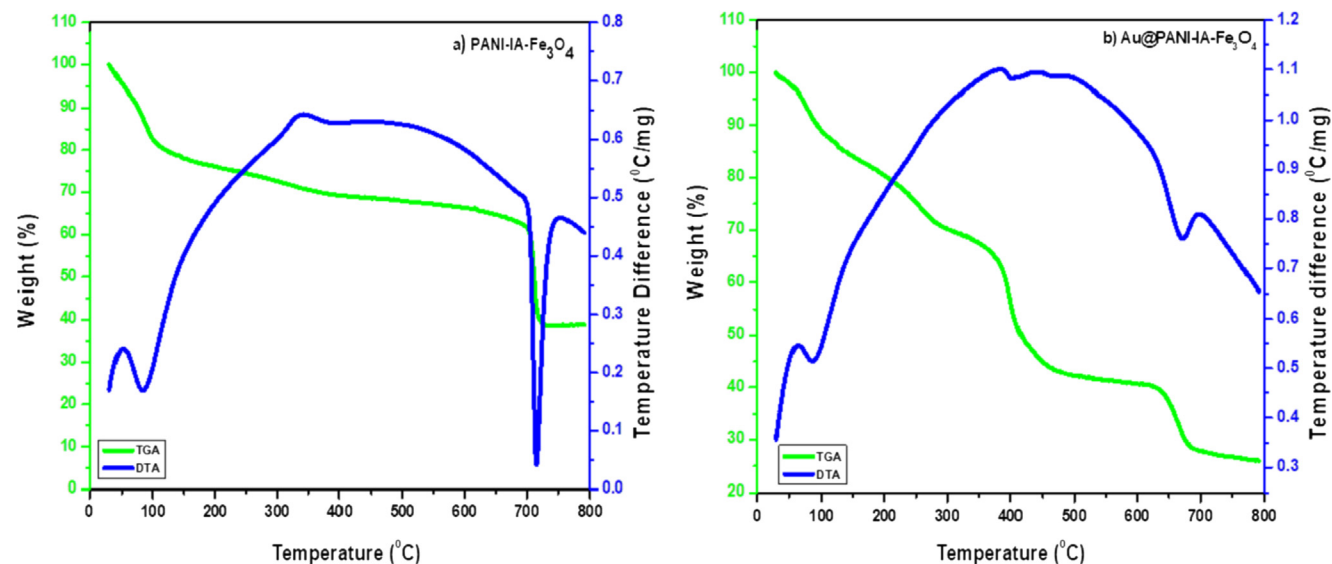

Fig. 2 TGA/DTA curves of (a) PANI–IA–Fe$_3$O$_4$ and (b) Au@PANI–IA–Fe$_3$O$_4$ magnetic nanocomposite.

THF/water and NMP/water (Zeghioud et al., 2015; Butoi et al., 2017). Hence, the prepared Au@PANI–IA–Fe_3O_4 were not diminished in any solvents that exposed the stability of the compound. The obtained results are shown in Table 2.

4.4. X-ray powder diffraction (XRD)

The crystallinity has been investigated through the XRD pattern. Fig. 3 shows the XRD spectra of PANI, PANI–IA–Fe_3O_4 and Au@PANI–IA–Fe_3O_4 nanocomposite. The main reflections correspond to a pseudo orthorhombic phase of PANI (Mirmohseni et al., 2012). The slight sharps peaks have been observed at 2θ of 15.36°, 20.65°, 25.22°, and 35.73° which representing the crystal planes of [0 1 1], [1 0 0], [1 1 0]and [2 0 0] of PANI, respectively Fig. 3a (Yin et al., 2019). The peak centered at 2θ of 25.22° could be attributed to periodicity perpendicular to the polymer chain of PANI (Hasik et al., 2001). Whereas, pure PANI, a broad amorphous peak has been observed at 2θ of 20.65° might due to the attribution of the conjugated polymer chain (Belaabed et al., 2012; Zhang et al., 2018). The diffractogram of PANI–IA–Fe_3O_4 magnetic nanocomposite has shown two peaks at 14.26° and 33.21° with a characteristic distance of 6.23 Å and 2.69 Å, respectively (Fig. 3b). The formation of PANI–IA–matrix was also supported by the comparison of PANI and PANI–IA (Zeghioud et al., 2015). The Fig. 3b, shows peaks at 2θ of 21.45°, 32.98°, 42.88°, 53.89°, 64.35° and 84.19° could be indexed as [h k l] to [2 2 0], [3 1 1], [4 0 0], [4 2 2], [4 4 0] and [5 1 1] planes of face-centered cubic (fcc) of Fe_3O_4 observed in PANI-IA-Fe_3O_4 nanocomposite (Mu et al., 2017; Minisy et al., 2018). The above results Au@PANI–IA–Fe_3O_4 nanocomposite after the formation of gold nanoparticles over its surface was performed well. The four main diffraction lines were observed at 2θ of 38.47, 44.71, 64.35 and 77.96 that can be indexed with (h k l) crystallographic planes to [1 1 1], [2 0 0], [2 2 0] and [3 1 1] with related to FCC gold crystals. The formation of AuNPs on the PANI–IA–Fe_3O_4 magnetic nanocomposite of

XRD was also well supported to FT-IR results (Punuri et al., 2012; Ayad et al., 2017).

4.5. SEM–EDX studies of Au@PANI–IA–Fe_3O_4 nanocomposite

The surface morphology and the particle sizes of Au@PANI–IA–Fe_3O_4 size distribution of the magnetic nanocomposite were identified using SEM/EDX. Fig. 4a show the typical SEM image of Au@PANI–IA–Fe_3O_4 magnetic nanocomposite. The SEM images reveal the nanostructure of the synthesized nanocomposite and the triangle and bar shape of the Fe_3O_4–Au nanostructures (without aggregation) on PANI – IA matrix with a particle size of about 20 μm (Ayad et al., 2017; Duc Quan et al., 2019).

The energy dispersive X-ray analysis of gold nanoparticles in the PANI–IA–Fe_3O_4 nanocomposite has shown in Fig. 4b. The Au@PANI–IA–Fe_3O_4 magnetic nanocomposite has shown an optical absorption peak at ~2.0 keV, which is a typical absorption of metallic gold nanoparticles (Duc Quan et al., 2019; Elavazhagan et al., 2011). The obtained result reveals the elemental composition and confirmed the presence of C, O, Fe, and Au in Au@PANI–IA–Fe_3O_4 nanocomposite. The embedded $HAuCl_4$ was successfully reduced into AuNPs and it has supported the Au signals. The gold nanoparticles peak was obtained at 2 Kev with 0.29% gold, 46.73% carbon, 10.485% iron, and 42.495% oxygen (Fig. 4b). There are no impurity peaks has been investigated which is support the purity of gold nanoparticles (Chitra et al., 2018). The distribution of iron and Au in Au@PANI–IA–Fe_3O_4 magnetic nanocomposite was demonstrated via elemental mapping technique (Fig. 4b). The obtained results were indicated that the Fe_3O_4 and AuNPs over PANI-IA matrix.

4.6. Transmission electron microscopy

The TEM analysis was used to identify the structure of PANI–IA–Fe_3O_4 and Au@PANI–IA–Fe_3O_4 magnetic nanocomposite. A uniform distribution of gold nanoparticles within the nanocomposite matrix were observed in different TEM images. The TEM images of PANI–IA–Fe_3O_4 and Au@PANI–IA–Fe_3O_4 nanocomposite (Fig. 5a & b) have shown the dispersion of Fe_3O_4 and AuNPs through PANI–IA matrix with low aggregation at high magnification resolution 20 nm. A uniform distribution of Fe_3O_4–Au nanostructures demonstrated with low aggregation to some extent was examined. The TEM image of Au@PANI–IA–Fe_3O_4 nanocomposite has been observed in Fig. 5b. The crystalline AuNPs as the lattice fringes spacing is 50 nm, which is consistent with the crystal structure of Fe_3O_4 formation. The typical HRTEM image were 20 nm reveal the crystal structure of Au nanoparticles within the polymer matrix in Fig. 5c. Hence, Au@PANI–IA–Fe_3O_4 magnetic nanocomposites with small size could reveled larger surfaces (20 nm and 50 nm) and a more competent active center, which is a favorite of bacterial activity (Min et al., 2007). Chitra et al, Similar to our observation, the indole-3-acetic acid-based nanocomposite systems. The selected area via electron diffraction (SAED) of Au@PANI–IA–Fe_3O_4 nanocomposite and the arrays with bright circles supported the crystallinity of these nanoparticles
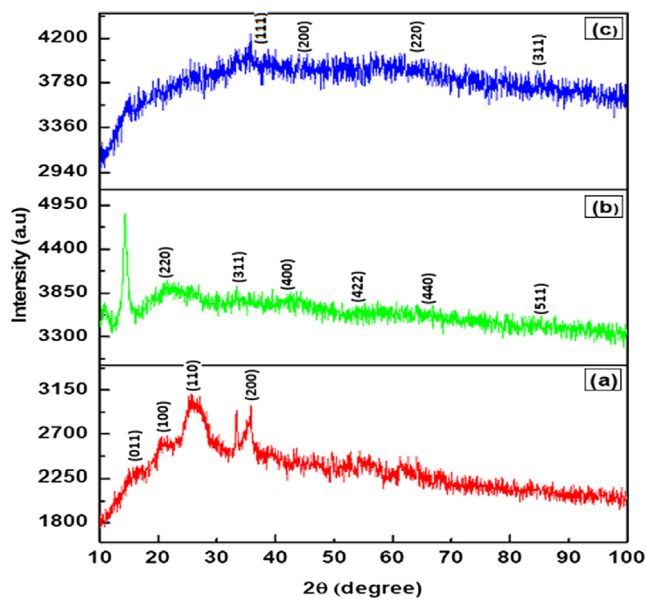

Fig. 3 XRD patterns of the prepared (a) PANI, (b) PANI–IA–Fe_3O_4, and (c) Au@ PANI–IA–Fe_3O_4 magnetic nanocomposites.
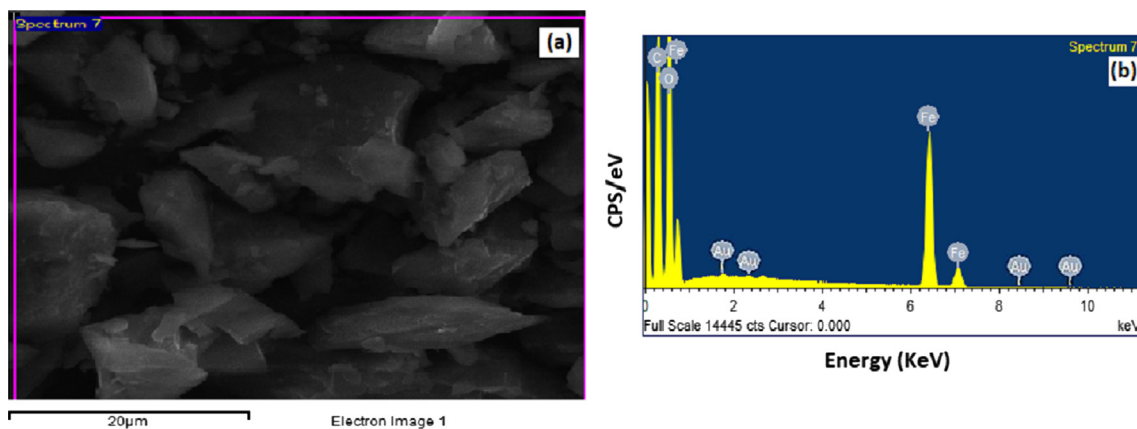
Fig. 4 SEM micrographs of (a) Au@PANI–IA–Fe₃O₄ and EDX images of (b) Au@PANI–IA–Fe₃O₄ magnetic nanocomposite.
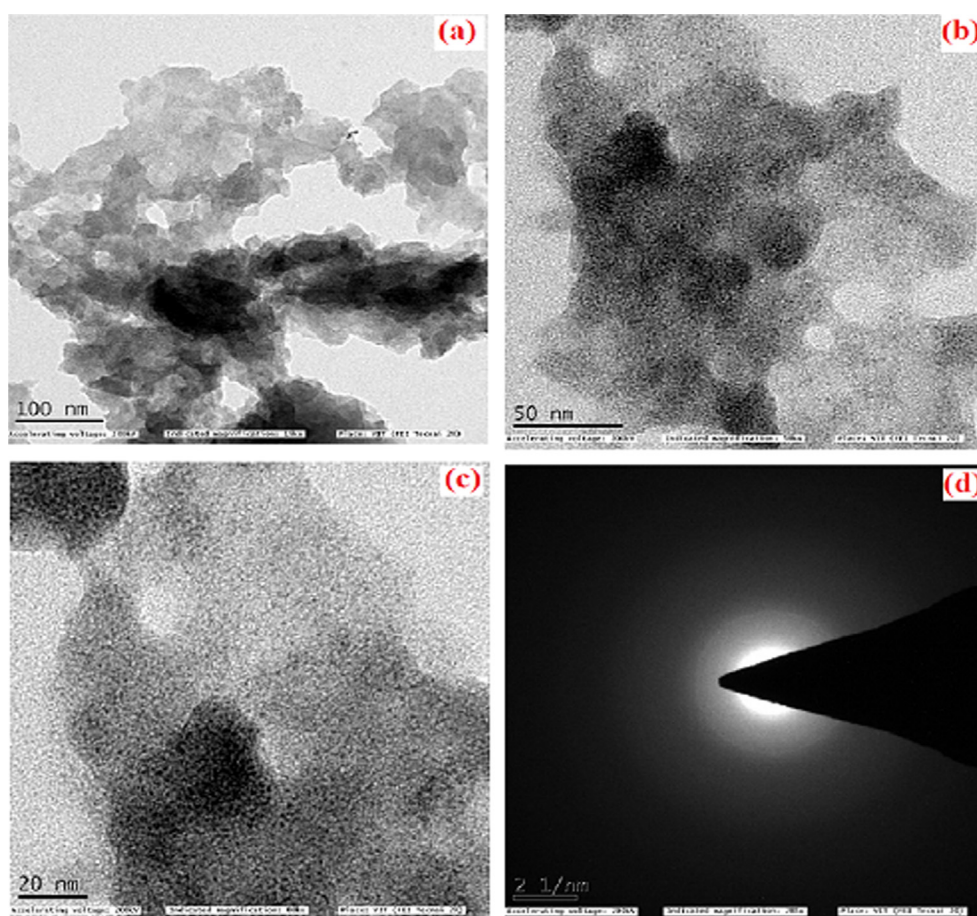

Fig. 5 TEM images of PANI–IA–Fe₃O₄ magnetic nanocomposite (a), Au@PANI–IA–Fe₃O₄ magnetic nanocomposite (b), HRTEM of Au@PANI–IA–Fe₃O₄ magnetic nanocomposite (c), and SAED of Au@PANI–IA–Fe₃O₄ magnetic nanocomposite (d).

has showed Fig. 5d. (Chitra et al., 2018). The magnetic, biological and thermal behavior of Au@PANI–IA–Fe₃O₄ might be due to the presence of AuNPs crystal in different sizes and shapes to account for the polymer matrix.

4.7. Magnetic properties (VSM)

Magnetization measurements of PANI–IA–Fe₃O₄ and Au@PANI–IA–Fe₃O₄ magnetic nanocomposites were done by vibrating sample magnetometer (VSM) at room temperature. Fig. 6. Shows the images of magnetization of nanocomposites para, dia, and super paramagnetic materials, when the applied magnetic field is removed, they should exhibit no coercivity and remanence. Paramagnetic materials have a linear relationship between magnetization (M) and applied filed (H) with a positive slope. The suggesting paramagnetic character with a saturation magnetization of PANI–IA–Fe₃O₄ and Au@PANI–IA–Fe₃O₄ values were found to be 0.925 emu/g
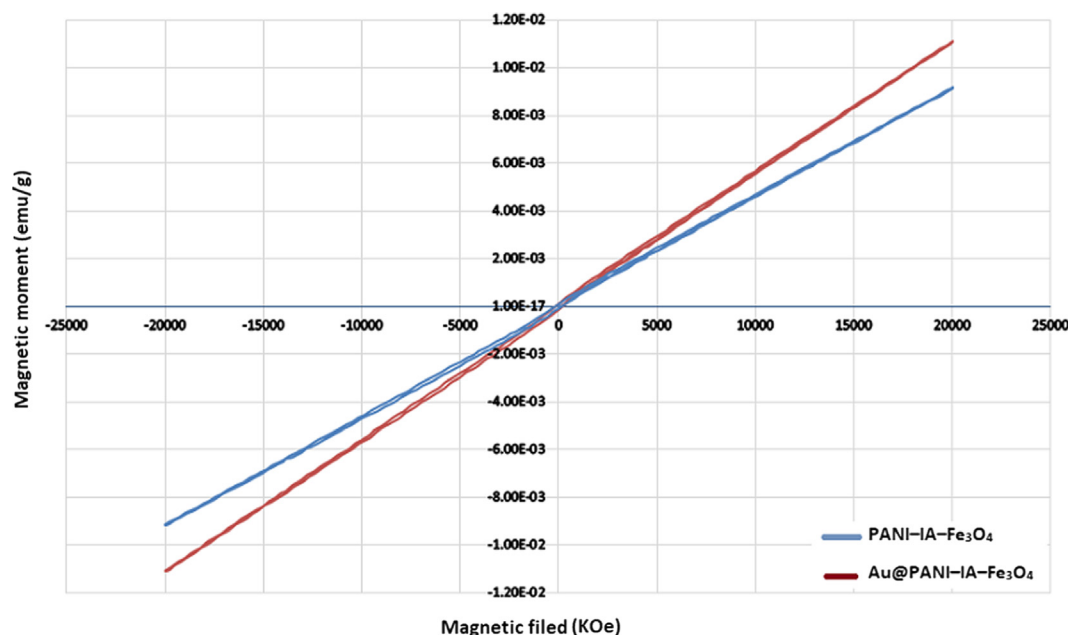
Fig. 6   Magnetization curves of PANI–IA–Fe$_3$O$_4$ and Au@PANI–IA–Fe$_3$O$_4$ magnetic nanocomposite.

and 1.140 emu/g. The net magnetization of the PANI based nanocomposite has been reduced due to a further reduction in the magnetization. The prepared PANI based complex exhibits paramagnetic character, which indicates it could act as a potent MRI positive contrast agent (Thenmozhi et al., 2015; Azizian et al., 2012). The obtained paramagnetic character is due to the interactions of ferrite and polymeric matrix with the PANI-IA prepared ferrite. Donescu et al, also been examined the one without similar PANI-based ferrite complex (Donescu et al., 2017). This behavior of the M−H curves is a well-known characteristic of materials with paramagnetic properties.

4.8. Antibacterial activity of Au@PANI–IA–Fe$_3$O$_4$ nanocomposite

The *in-vitro* antibacterial activity of Au@PANI–IA–Fe$_3$O$_4$ nanocomposite tested against *Staphylococcus aureus* (gram + ve) and *Escherichia coli* (gram −ve) pathogens Mueller-Hinton agar (MHA) plates test as shown in Fig. 7. The synthesized AuNPS embedded Au@PANI–IA–Fe$_3$O$_4$ magnetic nanocomposite has been exhibited good antibacterial activity against two pathogens compared to Ciproflaxin (Fig. 7a-b). This could be related to a more antibacterial feature of AuNPs, largely due to the inert chemical nature of gold present within the nanocomposite (Zhou et al., 2012). The Ciproflaxin was chosen as a broad-spectrum antibiotic standard. The zone of inhibition of itaconic acid based nanocomposite against pathogens was determined with varying concentrations of 50 µg, 100 µg, 250 µg and 500 µg (Chitra et al., 2018; Sakthivel et al., 2018). The zone of inhibition of Au@PANI–IA–Fe$_3$O$_4$ has been exhibited anti-bacterial efficacy towards *S. aureus* (gram + ve) was 10 mm, 11 mm, 12 mm and 14 mm for 50 µg, 100 µg, 250 µg, 500 µg respectively. The obtained results did not support the antibacterial zone of inhibition against pathogens and it mainly depends on the concen-

tration of IA. The synthesized magnetic nanocomposite has shown better sensitivity against *S.aureus* (gram + ve) bacterial strains. Whereas, Au@PANI–IA–Fe$_3$O$_4$ magnetic nanocomposite did not exhibit a significant antibacterial effect observed against *E. coli* (gram −ve) bacteria. Sakthivel et al and Kenawy et al, also mentioned the positively charged antibacterial polymers tendency to bind with (gram −ve) bacteria and there by splitting of negatively charged bacterial membranes (Sakthivel et al., 2018; Kenawy et al., 2007). Hence, the prepared Au@PANI–IA–Fe$_3$O$_4$ based nanocomposite has been enhanced after the incorporation of AuNPs with anionic charged polymers against + ve pathogen (*S.aureus*) (Pulat et al., 2008). The Au@PANI–IA–Fe$_3$O$_4$ magnetic nanocomposite has been revealed a better antibacterial property. This could be attributed to the combined antibacterial effect of Au and IA in Au@PANI–IA–Fe$_3$O$_4$ magnetic nanocomposite.

4.9. Antifungal activity of Au@PANI–IA–Fe$_3$O$_4$ nanocomposite

In recent years anti-fungal activity based polymeric material has been focused in different biomedical applications. The most common species of *Aspergillus nigeris* has been derived from the genus Aspergillus. In general, some fruits and vegetables have been affected on the surface of fruits which causes black mould disease. Whereas, ear infections and serious lung disease have been observed in humans. The *Candida albicans* originated from the Candida genus has also produced various disease viz., candidiasis, fungemia, morbidity, etc. Fig. 8. has shown the antifungal activity of gold anchor PANI–IA–Fe$_3$O$_4$ nanocomposites with a different zone. Here, two pathogens such as *Aspergillus niger* and *Candida albicans* were utilized to observe the antifungal activity. The Ciproflaxin (20 µg/well) was preferred as a positive control. The antifungal zone of inhibition has been examined, with respect to different Au@PANI–IA–Fe$_3$O$_4$ nanocomposite concentrations viz., 50 µg, 100 µg, 250 µg, and 500 µg. The antifungal
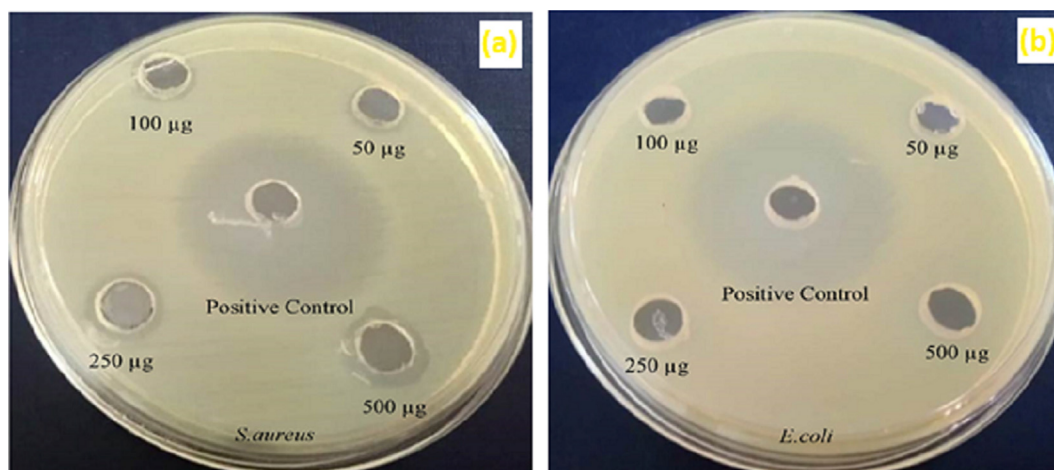
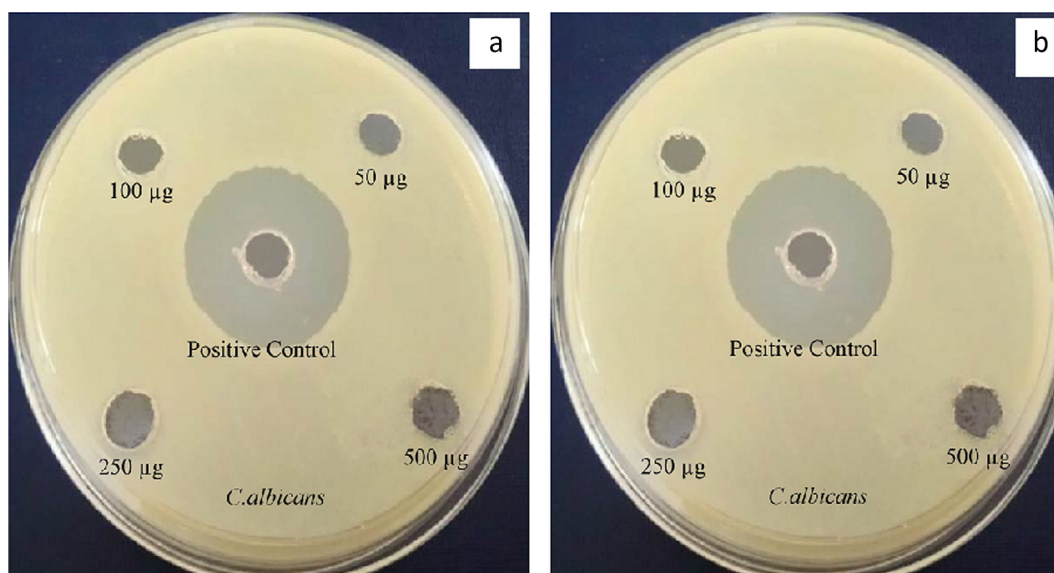Fig. 7   Antibacterial effect of Au@PANI–IA–Fe₃O₄ magnetic nanocomposite.

Fig. 8   Antifungal activity of Au@PANI–IA–Fe₃O₄ magnetic nanocomposite.

activity of gold anchor PANI–IA–Fe₃O₄ nanocomposites of *C. albicans* was found to 1 mm, 2 mm, 3 mm, & 7 mm respectively. The achieved results have clearly shown that the gold anchor PANI–IA–Fe₃O₄ nanocomposite as a better antifungal activity. This might be due to the increasing stoichiometric amount and hydrophilic nature of IA in the polymeric nanocomposite (Tomic et al., 2009; Zhang et al., 2013). However, no such kind of the microbial growth was observed against *A. Niger*. Sakthivel et al, has also been studied using Itaconic acid based pH-sensitive hydrogels systems (Sakthivel et al., 2018). Hence, the results imply gold anchor PANI based magnetic nanocomposite has a significant inhibition activity against *C. albicans*.

5. Conclusion

In general, magnetic nanocomposites of different feed compositions were synthesized in a simple and eco-friendly route.

Piper betel (leaf extract) was used for the fabrication of AuNPs. incorporation of AuNPs into PANI–IA–Fe₃O₄ magnetic nanocomposites resulted in gold anchor nanocomposites. The different IA/PANI based composites were developed. The following FT-IR, XRD, TGA/DTA, SEM, EDX, TEM, and VSM also been done. Further, antibacterial and antifungal activity has also been studied. In general, AuNPs surface-treated nanocomposite properties were found to be excellent overall, compared to the untreated ones. Improved thermal stability was examined for AuNPs treated nanocomposite. The present investigation clearly suggests that the magnetic nanocomposites could also be potential candidates for medial and industrial application when they are surface modified with AuNPs.

Declaration of Competing Interest

The authors declared that there is no conflict of interest.

Acknowledgments

References

Ayad, M.M., Amer, W.A., Kotp, M.G., Minisy, I.M., Rehab, A.F., Kopecky, D.S., Fitl, P., 2017. Synthesis of silver-anchored polyaniline–chitosan magnetic nanocomposite: a smart system for catalysis. RSC Adv. 7, 18553. https://doi.org/10.1039/c7ra02575k.

Ayad, M.M., Amer, W.A., Whdan, M., 2012. In situ polyaniline film formation using ferric chloride as an oxidant. J. Appl. Polym. Sci. 125, 2695–2700. https://doi.org/10.1002/app.36584.

Azizian, G., Riyahi Alam, N., Haghgoo, S., Reza Moghimi, H., Zohdiaghdam, R., Rafiei, B., Gorji, E., 2012. Synthesis route and three different core-shell impacts on magnetic characterization of gadolinium oxide-based nanoparticles as new contrast agents for molecular magnetic resonance imaging. Nanoscale Res. Lett. 7, 549. https://doi.org/10.1186/1556-276X-7-549.

Barrios, E.M., Mujica, G.A., Velasquez, C.L., Martınez, Y., 2006. Studies of the presence of dicarboxylic acids in the electrochemical synthesis of poly (aniline): Case poly (itaconic acid). J. Electroanal. Chem. 586, 128–135. https://doi.org/10.1016/j.jelechem.2005.09.022.

Belaabed, B., Wojkiewicz, J.L., Lamouri, S., El Kamchi, N., Lasri, T., 2012. Synthesis and characterisation of hybrid conducting composites based on polyaniline/magnetite fillers with improved microwave absorption properties. J. Alloy. Compd. 527, 137–144. https://doi.org/10.1016/j.jallcom.2012.02.179.

Butoi, B., Groza, A., Dinca, P., Balan, A., Barna, V., 2017. Morphological and structural analysis of polyaniline and poly(o-anisidine) layers generated in a DC glow discharge plasma by using an oblique angle electrode deposition configuration. Polymers 9, 732. https://doi.org/10.3390/polym9120732.

Chen, G., Cui Daxiang, C., 2012. Functionalized gold nanorods for tumour imaging and targeted therapy. Cancer Biol. Med. 9, 221–233. https://dx.doi.org/10.7497%2Fj.issn.2095-3941.2012.04.002.

Chitra, G., Franklin, D.S., Sudarsan, S., Sakthivel, M., Guhanathan, S., 2018. Noncytotoxic silver and gold nanocomposite hydrogels with enhanced antibacterial and wound healing applications. Polym. Eng. Sci. 58, 2133–2142. https://doi.org/10.1002/pen.24824.

Ciric-Marjanovic, G., 2013. Recent advances in polyaniline research; polymerization mechanisms, structural aspects, properties and applications. Synth. Met. 177, 1–47. https://doi.org/10.1016/j.synthmet.2013.06.004.

Daniel, M.C., Astruc, D., 2004. Gold nanoparticles: assembly, supramolecular chemistry, quantum-size-related properties, and applications toward biology, catalysis, and nanotechnology. Chem. Rev. 104, 293–346. https://doi.org/10.1021/cr030698.

Das, M., Shim, K.H., An, S.S.A., Yi, D.K., 2011. Review on gold nanoparticles and their applications. Toxicol. Environ. Health Sci. 3, 193–205. https://doi.org/10.1007/s13530-011-0109-y.

Donescu, D., Claudiu Fierascu, R., Ghiurea, M., Manaila-Maximean, D., Nicolae, C., Somoghi, R., Spataru, C., Stanica, N., Raditoiu, V., Vasile, E., 2017. Synthesis and magnetic properties of inverted core-shell polyaniline-ferrite composite. Appl. Surf. Sci. 414, 8–17. https://doi.org/10.1016/j.apsusc.2017.04.061.

Duc Quan, L., Huu Dang, N., Hoang, T., Tu, Ngoc PhuongLinh, V., Thi Mong Thy, L., Minh Nam, H., Thanh Phong, M., Huuhieu, N., 2019. Preparation of magnetic iron oxide/graphene aerogel nanocomposites for removal of bisphenol A from water. Synthetic Metals. 255. https://doi.org/10.1016/j.synthmet.2019.116106.

Elavazhagan, T., Arunachalam, K.D., 2011. Memecylonedule leaf extract mediated green synthesis of silver and gold nanoparticles. Int. J. Nanomed. 6, 1265–1278. https://doi.org/10.2147/IJN.S18347.

Geng, P., Cao, S., Guo, X., Ding, J., Zhang, S., Zheng, M., Pang, H., 2019. Polypyrrole indexing hollow metal-organic framework composites for lithium-sulfur batteries. J. Mater. Chem. A 7, 19465–19470. https://doi.org/10.1039/C9TA05812E.

Geng, P., Zheng, S., Tang, H., Zhu, R., Zhang, L., Cao, S., Xue, H., Pang, H., 2018. Transition metal sulfides based on graphene for electrochemical energy storage. Adv. Energy Mater. 1703259, 1–26. https://doi.org/10.1002/aenm.201703259.

Ghaffari-Moghaddam, M., Eslahi, M., 2014. Synthesis, characterization and antibacterial properties of a novel nanocomposite based on polyaniline/polyvinyl alcohol/Ag. Arabian J. Chem. 7, 846–855. https://doi.org/10.1016/j.arabjc.2013.11.011.

Gupta, A.K., Gupta, M., 2005. Synthesis and surface engineering of iron oxide nanoparticles for biomedical applications. Biomaterials 26, 3995–4021. https://doi.org/10.1016/j.biomaterials.2004.10.012.

Hasan, M., Ansari, M.O., Cho, M.H., 2015. Electrical conductivity, optical property and ammonia sensing studies on HCl Doped Au@polyaniline nanocomposites. Electron. Mater. Lett. 11, 1–6. https://doi.org/10.1007/s13391-014-4200-9.

Hasik, M., Drelinkiewicz, A., Wenda, E., Paluszkiewicz, C., Quillard, S.J., 2001. FTIR spectroscopic investigation of polyaniline derivatives-palladium systems. J. Mol. Struct. 596, 89–99. https://doi.org/10.1016/S0022-2860(01)00694-9.

Heeger, A.J., 2001. Semiconducting and metallic polymers: the fourth generation of polymeric materials. J. Phys. Chem. B 105, 8475–8491. https://doi.org/10.1002/1521-3773(20010716)40:14%3C2591::AID ANIE2591%3E3.0.CO;2-0.

Ibrahim, K., Khalid, S., Idrees, K., 2017. Nanoparticles: Properties, applications and Toxicities. Arabian J. Chem. 7, 908–931. https://doi.org/10.1016/j.arabjc.2017.05.011.

Isiklan, N., Kursun, F., Inal, M., 2010. Graft copolymerization of itaconic acid onto sodium alginate using benzoyl peroxide. Carbohydr. Polym. 79, 665–672. https://doi.org/10.1016/j.carbpol.2009.09.021.

Jolanda, S., Dania, M., Caroline, M., Ciaran Manus Maguire, C.M., Moustaoui, H., Casale, S., Volkov, Y., Prina-Mello, A., 2016. Targeted polyethylene glycol gold nanoparticles for the treatment of pancreatic cancer: from synthesis to proof of concept in vitro studies. Int. J. Nanomed. 11, 791–822. https://doi.org/10.2147/IJN.S97476.

Kalaivasan, N., Syed Shafi, S., 2012. Enhancement of corrosion protection effect in mechanochemically synthesized Polyaniline/MMTclay nanocomposites. Arabian J. Chem. 10, 127–133. https://doi.org/10.1016/j.arabjc.2012.06.018.

Kenawy, E.R., Worley, S.D., Broughton, R., 2007. The chemistry and applications of antimicrobial polymers: a state-of-the-art review. BioMacromolecules 8, 1359–1384. https://doi.org/10.1021/bm061150q.

Khan, Z., Bashir, O., Hussain, J.I., Kumar, S., Ahamed, R., 2012. Effects of ionic surfactants on the morphology of silver nanoparticle using paan(piper betel) leaf petiole extract. Colloids Surf., B 98, 85–90. https://doi.org/10.1016/j.colsurfb.2012.04.033.

Khilari, S., Pandit, S., Varanasi, J.L., 2015. Bifunctional manganese ferrite/polyaniline hybrid as electrode material for enhanced energy recovery in microbial fuel cell. ACS Appl. Mater. Interfaces 7, 20657–20666. https://doi.org/10.1021/acsami.5b05273.

Khutale, G.V., Casey, A., 2017. Synthesis and characterization of a multifunctional gold-doxorubicin nanoparticle system for pH triggered intracellular anticancer drug release. Eur. J. Pharm. Biopharm. 119, 372–380. https://doi.org/10.1016/j.ejpb.2017.07.009.

Lee, S., Cha, E.J., Park, K., Lee, S.Y., Hong, J.K., Sun, I.C., Kim, S. Y., Choi, K., Kwon, I.C., Kim, K., 2008. A near-infrared-fluorescence-quenched gold-nanoparticle imaging probe for

in vivo drug screening and protease activity determination. Angew. Chem. 47, 2804–2807. https://doi.org/10.1002/anie.200705240.

Li, D., Xu, H., Jiao, L., Jiang, H., 2019. Metal-organic frameworks for catalysis: State of the art, challenges, and opportunities. J. Energy Chem. 1,. https://doi.org/10.1016/j.enchem.2019.100005 100005.

Liu, C., Xu, Y., Wu, L., 2015. Fabrication of core–multi shell MWCNT/Fe$_3$O$_4$/PANI/Au hybrid nanotubes with high-performance electromagnetic absorption. J. Mater. Chem. A 3, 10566–10572. https://doi.org/10.1039/C5TA01973G.

Liu, H.L., Ko, S.P., Wu, J.H., Jung, M.H., Min, J.H., Lee, J.H., 2007. One-pot polyol synthesis of mono size PVP-coated sub-5nm Fe$_3$O$_4$ nanoparticles for biomedical applications. J. Magn. Magn. Mater. 310, 815–817. https://doi.org/10.1016/j.jmmm.2006.10.776.

Manawwer, A., Anees, A.A., Rafi Shaik, M., Naser, M.A., 2013. Optical and electrical conducting properties of Polyaniline/Tin oxide nanocomposite. Arabian J. Chem. 6, 341–345. https://doi.org/10.1016/j.arabjc.2012.04.021.

Min, S., Wang, F., Han, Y., 2007. An investigation on synthesis and photocatalytic activity of polyaniline sensitized nanocrystalline TiO$_2$ composites. J. Mater. Sci. 42, 9966–9972. https://doi.org/10.1007/s10853-007-2074-z.

Minisy, M., Salahuddin, A., Ayad, M.M., 2018. Chitosan/polyaniline hybrid for the removal of cationic and anionic dyes from aqueous solutions. J. Appl. Polym. Sci. 47056, 1–12. https://doi.org/10.1002/app.47056.

Mirabedini, A., Foroughi, J., Wallace, G.G., 2016. Developments in conducting polymer fibres: from established spinning methods toward advanced applications. RSC Adv. 6, 44687–44716. https://doi.org/10.1039/C6RA05626A.

Mirmohseni, A., Seyed Dorraji, M.S., Hosseini, M.G., 2012. Influence of metal oxide nanoparticles on pseudocapacitive behavior of wet-spun polyaniline-multiwall carbon nanotube fibers. Electrochim. Acta 70, 182–192. http://dx.doi.org/10.1016%2Fj.electacta.2012.03.100.

Mody, V.V., Siwale, R., Singh, A., Mody, H.R., 2010. Introduction to metallic nanoparticles. J. Pharm. Bio allied Sci. 2, 282–289. https://doi.org/10.4103/0975-7406.72127.

Mondal, P., Guo, C., Yarger, L.J., 2020. Water soluble gold-polyaniline nanocomposite: A substrate for surface enhanced Raman scattering and catalyst for dye degradation. Arabian J. Chem. 13, 4009–4018. https://doi.org/10.1016/j.arabjc.2019.05.004.

Mu, B., Tang, J., Zhang, L., Wang, A., 2017. Facile fabrication of superparamagnetic graphene/ polyaniline/Fe$_3$O$_4$ nanocomposites for fast magnetic separation and efficient removal of dye. Sci. Rep. 7, 5347. https://doi.org/10.1038/s41598-017-05755-6.

Mu, B., Wang, A., 2015. One-pot fabrication of multifunctional superparamagnetic attapulgite/Fe$_3$O$_4$/polyaniline nanocomposites served as an adsorbent and catalyst support. J. Mater. Chem. A 3, 281–289. https://doi.org/10.1039/C4TA05367B.

Murthy, N., Thng, Y.X., Schuck, S., Xu, M.C., Frechet, J.M.J., 2002. A novel strategy for encapsulation and release of proteins: Hydrogels and microgels with acid-labile acetal cross-linkers. J. Am. Chem. Soc. 124, 12398–12399. https://doi.org/10.1021/ja026925r.

Palaniappan, S., John, A., 2008. Polyaniline materials by emulsion polymerization pathway. Prog. Polym. Sci. 33, 732–758. https://doi.org/10.1016/j.progpolymsci.2008.02.002.

Peymanfar, R., Norouzi, F., Javanshir, S., 2019. Preparation and characterization of one-pot PANi/Fe/Fe$_3$O$_4$ /Fe$_2$O$_3$ nanocomposite and investigation of its microwave, magnetic and optical performance. Synth. Met. 252, 40–49. https://doi.org/10.1016/j.synthmet.2019.04.008.

Pulat, M., Eksi, H., Abbasoglu, U., 2008. Fluconazole release from hydrogels including acrylamide-acrylic acid-itaconic acid and their microbiological interactions. J. Biomater. Sci. Polym. Ed. 19, 193–205. https://doi.org/10.1163/156856208783432480.

Punuri, J.B., Sharma, P., Sibyala, S., Tamuli, R., Bora, U., 2012. Piper betle-mediated green synthesis of biocompatible gold nanoparti-

cles. Int. Nano Lett. 2, 1–9. https://doi.org/10.1186/2228-5326-2-18.

Pyarasani, R.D., Jayaramudu, T., John, A., 2018. Polyaniline-based conducting hydrogels. J. Mater. Sci. 54, 974–996. https://doi.org/10.1007/s10853-018-2977-x.

Qi, C., Zheng, J., 2015. Novel nonenzymatic hydrogen peroxide sensor based on Fe$_3$O$_4$/PPy/Ag nanocomposites. J. Electroanal. Chem. 747, 53–58. https://doi.org/10.1016/j.jelechem.2015.04.004.

Ramji, N., Ramji, N., Iyer, R., Chandrasekaran, S., 2002. Phenolic antibacterial from Piper betle in the prevention of halitosis. J. Ethnopharmacol. 83, 149–152. https://doi.org/10.1016/S0378-8741(02)00194-0.

Sakthivel, M., Franklin, D.S., Sudarsan, S., Chitra, G., Sridharan, T.P., Guhanathan, S., 2018. Investigation on pH/salt-responsive multifunctional itaconic acid based polymeric biocompatible, antimicrobial and biodegradable hydrogels. React. Funct. Polym. 122, 9–21. https://doi.org/10.1016/j.reactfunctpolym.2017.10.021.

Sampreeth, T., Al-Maghrabi, M.A., Bahuleyan, B.K., Ramesan, M.T., 2018. Synthesis, characterization, thermal properties, conductivity and sensor application study of polyaniline/cerium-doped titanium dioxide nanocomposites. J. Mater. Sci. 53, 591–603. https://doi.org/10.1007/s10853-017-1505-8.

Suganthy, N., Sri Ramkumar, V.P., Ugazhendhi, A., Benelli, G., Archunan, G., 2018. Biogenic synthesis of gold nanoparticles from Terminalia arjuna bark extract: Assessment of safety aspects and neuroprotective potential via antioxidant, anticholinesterase, and anti-amyloidogenic effects. Environ. Sci. Pollut. Res. 25, 10418–10433. https://doi.org/10.1007/s11356-017-9789-4.

Sun, H., Zhu, X., Zhang, L., Zhang, Y., Wang, D., 2010. Capture and release of genomic DNA by PEI modified Fe$_3$O$_4$/Au nanoparticles. Mater. Sci. Eng., C 30, 311–315. https://doi.org/10.1016/j.msec.2009.11.005.

Teng, Z., Lv, H., Wang, C., Xue, H., Pang, H., Wang, G., 2017. Bandgap engineering of ultrathin graphene-like carbon nitride nanosheets with controllable oxygenous functionalization. Carbon 113, 63–75. https://doi.org/10.1016/j.carbon.2016.11.030.

Thenmozhi, M., Pooja, R., Nisha, P.R., Swaminathan, S., Uma Maheswari, K., 2015. Evaluation of quercetin-gadolinium complex as an efficient positive contrast enhancer for magnetic resonance imaging. RSC Adv. 5, 86967. https://doi.org/10.1039/C5RA16405B.

Tomic, S.L., Dimitrijevic, S.I., Marinkovic, A.D., Najman, S., Filipovic, J.M., 2009. Synthesis and characterization of poly(2-hydroxyethyl methacrylate/itaconic acid) copolymeric hydrogels. Polym. Bull. 63, 837–851. https://doi.org/10.1007/s00289-009-0123-2.

Unal, B., Toprak, M.S., Durmus, Z., Sozeri, H., Baykal, A., 2010. Synthesis, structural and conductivity characterization of alginic acid–Fe$_3$O$_4$nanocomposite. J. Nanopart. Res. 12, 3039–3048. https://doi.org/10.1007/s11051-010-9898-1.

Velickovic, S.J., Dzunuzovic, E.S., Griffiths, P.C., 2008. Polymerization of itaconic acid initiated by a potassium persulfate/N, N-dimethylethanolamine system. J. Appl. Polym. Sci. 26, 3275–3282. https://doi.org/10.1002/app.28843.

Vijayanand, R.S., Vivekanandan, J., Mahudeswaran, A., Jayaprakasam, R., 2016. Synthesis and characterization of aniline and 4-fluoroaniline conducting copolymer composites doped with silver nanoparticles. Macromol. Symposia 362, 65–72. https://doi.org/10.1002/masy.201400270.

Wang, D., He, J., Rosenzweig, N., Rosenzweig, Z., 2004. Superparamagnetic Fe$_2$O$_3$ beads– CdSe/ZnS quantum dots core-shell nanocomposite particles for cell separation. Nano Letters 4, 409–413. https://doi.org/10.1021/nl035010n.

Wang, S., Bao, H., Yang, P., Chen, G., 2008. Immobilization of trypsin in polyaniline coated nano-Fe$_3$O$_4$/carbon nanotube composite for protein digestion. Anal. Chim. Acta 612, 182–189. https://doi.org/10.1016/j.aca.2008.02.035.

Wang, Y., Zheng, H., Jia, L., Li, H., Li, T., Chen, K., Gu, Y., Ding, J., 2014. Synthesis and characterization of conductive and soluble itaconic acid doped polyaniline nanorods. J. Macromol. Sci., Part A 51, 619–624. https://doi.org/10.1080/10601325.2014.924834.

Xiao, X., Li, Q., Yuan, X., Xu, Y., Zheng, M., Pang, H., 2018. Ultrathin nanobelts as an excellent bifunctional oxygen catalyst: insight into the subtle changes in structure and synergistic effects of bimetallic metal-organic framework. Small Methods 1800240, 1–7. https://doi.org/10.1002/smtd.201800240.

Yin, T., Zhang, H., Yang, G., Wang, L., 2019. Polyaniline composite TiO2 nanosheets modified carbon paper electrode as a high performance bioanode for microbial fuel cells. Synth. Met. 252, 8–14. https://doi.org/10.1016/j.synthmet.2019.03.027.

Zeghioud, H., Lamouri, S., Safidine, Z., Belbachir, M., 2015. Chemical synthesis and characterization of highly soluble conducting polyaniline in mixtures of common solvents. J. Serb. Chem. Soc. 80, 917–931. https://doi.org/10.2298/JSC140719003Z.

Zhan, G., Huang, J., Du, M., Abdul-Rauf, I., Ma, Y., Li, Q., 2011. Green synthesis of Au–Pd bimetallic nanoparticles: Single-step bio reduction method with plant extract. Mater. Lett. 65, 2989–2991. https://doi.org/10.1016/j.matlet.2011.06.079.

Zhang, J., Guo, L., Meng, Q., Wang, W., Liu, M., Jin, Z., Zhao, K., 2018. Polyurethane and polyaniline foam-derived nickel oxide-incorporated porous carbon composite for high-performance supercapacitors. J. Mater. Sci. Electron. 53, 13156–13172. https://doi.org/10.1007/s10853-018-2583-y.

Zhang, J., Han, J., Wang, M., 2017. Fe_3O_4/PANI/MnO_2 core–shell hybrids as advanced adsorbents for heavy metal ions. J. Mater. Chem. A 5, 4058–4066. https://doi.org/10.1039/C6TA10499A.

Zhang, Q., Ye, J., Tian, P., Lu, X., Lin, Y., Zhao, Q., Ning, G., 2013. Ag/TiO_2 and Ag/SiO_2 composite spheres: synthesis, characterization and antibacterial properties. RSC Adv. 3, 9739–9744. https://doi.org/10.1039/C3RA40596F.

Zhou, Y., Kong, Y., Kundu, S., Cirillo, J.D., Liang, J.D., 2012. Antibacterial activities of gold and silver nanoparticles against Escherichia coli and bacillus Calmette-Guerin. J. Nanobiotechnol. 10, 19. https://doi.org/10.1186/1477-3155-10-19.